

Ice emission and the redshifts of submillimeter sources

C. C. Dudley

*Formerly: Naval Research Laboratory, Remote Sensing Division, 4555 Overlook Ave. SW,
Washington, DC 20375-5351, USA*

C.Christopher.Dudley.85@alum.dartmouth.org

M. Imanishi¹

National Astronomical Observatory, Mitaka, Tokyo 181-8588, Japan

and

P. R. Maloney

*Center for Astrophysics and Space Astronomy, University of Colorado, Boulder, CO
80309-0839, USA*

ABSTRACT

Observations at submillimeter wavelengths have revealed a population of sources thought to be at relatively large redshifts. The position of the 850 μm passband on the Rayleigh-Jeans portion of the Planck function leads to a maximum redshift estimate of $z \sim 4.5$ since sources will not retain their redshift independent brightness close to the peak of the Planck function and thus drop out of surveys. Here we review evidence that ice absorption is present in the spectra of local ultraluminous infrared galaxies which are often taken as analogs for the 850 μm source population. We consider the implication of this absorption for ice induced spectral structure at far infrared wavelengths and present marginal astronomical evidence that amorphous ice may have a feature similar to crystalline ice near 150 μm . Recent corroborative laboratory evidence is supportive of this conclusion. It is argued that early metal enrichment by pair instability SN may lead to a high ice content relative to refractory dust at high redshift and a fairly robust detection of ice emission in a $z = 6.42$ quasar is presented. It is further shown that ice emission is needed to understand the 450 μm sources observed in

¹Department of Astronomy, School of Science, Graduate University for Advanced Studies, Mitaka, Tokyo 181-8588

the GOODS-N field. We are thus encouraged to apply far infrared ice emission models to the available observations of HDF 850.1, the brightest submillimeter source in the *Hubble Deep Field*. We suggest that a redshift as large as 13 may need to be considered for this source, nearly a factor of three above the usual top estimate. Inclusion of the possibility of far infrared ice emission in the spectral energy distributions of model sources generally broadens the range of redshifts to be considered for submillimeter sources compared to models without ice emission.

Subject headings: galaxies: high redshift, formation — infrared: galaxies — galaxies: individual: IRAS 00188-0856, IRAS 14348-1447, QSO J1148+5251, HDF 850.1

1. Introduction

Sources discovered in surveys undertaken using 450/850 μm SCUBA camera mounted on the JCMT have a high number density per unit solid angle ($\sim 10^4 \text{ deg}^{-2}$; $S_{850} > 1 \text{ mJy}$; Sanders 2000; Wang et al. 2004) and are thought to trace the dust emission from sources at a range of redshifts. Sources brighter than 1 mJy which have Arp 220-like far infrared (FIR) spectral energy distributions (SEDs) are ultraluminous in the $h_{100} = 0.71$, $\Omega_m = 0.27$, and $\Omega_\Lambda = 0.73$ cosmology consistent with cosmic microwave background (CMB) and Type 1a SNe observations (Spergel et al. 2003; Nolte et al. 2004; Riess et al. 2004) unless they are at redshifts < 1 so that, thus far, submillimeter surveys do not detect “normal” galaxies at high redshift. This should be the case even for gravitational lens amplification up to a factor of 4 for 2 mJy limit surveys.

It is therefore a sensible approach to consider the properties of local ultraluminous infrared galaxies (ULIRGs; Sanders & Mirabel 1996) as a guide to understanding sources detected in submillimeter surveys with the proviso that the high redshift universe may not conserve these properties. It has already been noted that the number density of ULIRGs increases with redshift at a rate much larger than can be explained using geometric considerations alone (Kim & Sanders 1998) and deep field observations using the *Hubble Space Telescope* have found quite obvious morphological evolution at higher redshifts compared to local conditions (*e.g.* Brinchmann et al. 1998). While these particular evidences of evolution as a function of redshift do not directly speak to ULIRG SED evolution, they do suggest that this proviso cannot be lightly discounted.

Ice is present in the dense ISM of the Galaxy. It is observed to occur above a threshold depth of $A_V \sim 3$ within molecular clouds but is absent on the cloud edges and in the diffuse

(atomic/ionized) ISM (Whittet et al. 1988). Because ice is not exposed to star light, far infrared (FIR) emission from ice is not expected from quiescent clouds. The FIR emission from these ice bearing clouds arises from the first few ice-free A_V . To observe ice emission in the Galaxy, centrally heated sources are needed. If mid-infrared (MIR) radiation can illuminate the ice bearing grains so that they may be heated, then the FIR emission will be dominated by ice if the ice mantles provide a moderate fraction of the total grain volume. This FIR dominance is owing to greater FIR opacity of ice relative to silicate or carbonaceous grains. In the models presented by Aannestad (1975), a mantle-to-core volume ratio of 0.33 doubles the 60 μm opacity: a 10% increase in grain radius doubles the opacity!

Protostars in the Galaxy which are centrally heated turn out to be good sources for observing FIR ice emission (*e.g.* Dartois et al. 1998). And, there is mounting evidence that a significant fraction of local ULIRGs are also centrally heated (Dudley & Wynn-Williams 1997; Soifer et al. 2002; Imanishi & Dudley 2000; Imanishi & Maloney 2003; Imanishi et al. 2006a; Spoon et al. 2006) so that the FIR emission is a result of MIR heating. Thus, if ice is present in the FIR emitting regions, its effects on the FIR opacity may be important. This situation differs from what occurs in lower luminosity starburst galaxies where the FIR emission arises from the surfaces of molecular clouds which are heated by optical and far UV rather than MIR light. The interiors of the clouds, where ice presumably exists, are not strongly heated by the mainly FIR emission arising from their surfaces.

If submillimeter galaxies are similar to ULIRGs in more than just their luminosity, then they may also sometimes have FIR emission that is powered by MIR light. For redshift estimation the question of the similarity between submillimeter galaxies and local ULIRGs is as important as the differences that distinguish ULIRGs from their lower luminosity starburst counterparts.

Attempts to estimate redshifts for the submillimeter sources based on their radio fluxes could be guided by local ULIRG samples. For the 13 ULIRGs brighter than 5.24 Jy at 60 μm (Soifer et al. 1987; Sanders et al. 1995) available to the VLA, the mean logarithm of the ratio of FIR-to-20 cm radio flux is 0.22 dex larger than $q=2.43\pm0.19$ (Condon et al. 1991) for starburst galaxies when calculated using radio measurements reported by Condon et al. (1991) and Yun et al. (2001). While the mean differs at only the 1σ level, the dispersion of q is a factor 1.6 (in dex) larger than for the lower luminosity star forming galaxies. Using a different luminosity binning, Helou et al. (1985) report a similar trend in increased dispersion with increasing luminosity. The implication for redshift estimation is that the range of likely redshifts would increase when using ULIRG properties rather than starburst properties. And, a trend away from what is seen in local ULIRGs, say through more powerful starbursts at earlier times, could have complex implications for estimating redshifts of submillimeter

galaxies using radio observations.

However, broad limits on the redshift distribution derive from submillimeter observations alone where the relative infrequency of detecting $450\ \mu\text{m}$ emission leads to (weak) lower limits on the redshifts while the detections themselves at $850\ \mu\text{m}$ lead to upper limits since, barring extraordinary luminosities, the turnover from the Rayleigh-Jeans-like portion of the SED at high redshift leads to source fluxes dropping below survey detection limits.

Given the large potential effect of ice on the FIR opacity of submillimeter galaxies, we first review the evidence for the presence of ice in centrally heated ULIRGs and estimate an expected FIR SED for a case where FIR ice opacity can be expected to be dominant based on a rough abundance analysis. We then search for FIR ice spectral features in the available data on ULIRGs. We discuss why a high relative abundance of ice during the epoch of reionization might be expected and present somewhat firmer evidence for FIR ice emission in the $z = 6.42$ source QSO J1148+5251 than can yet be demonstrated for ULIRGs. We then take the submillimeter galaxy HDF 850.1 as an example to show how FIR ice emission allows a very large redshift estimate.

2. Ice in ULIRGs

2.1. Absorption

Observations of strong absorption features from refractory dust in ULIRGs trace dust that is cooler than the temperature of a blackbody emitting at the wavelength of the feature: $\sim 300\ \text{K}$ for the $10\ \mu\text{m}$ silicate feature and $\sim 150\ \text{K}$ for the $20\ \mu\text{m}$ silicate feature for example. Thus, $20\ \mu\text{m}$ silicate features are weak in ULIRGs compared to $10\ \mu\text{m}$ features owing to the dust radial temperature gradient. Ice absorption, on the other hand, should only occur in the cooler outer regions of the dust envelope and so may show the same relative feature strengths found in the laboratory unless the absorbing covering factor is a strong function of the emitting source’s wavelength dependent size (buried source radius $r \approx 0.8(\frac{L}{10^{12}L_{\odot}})^{0.5}(\frac{\lambda}{3\mu\text{m}})^2\ \text{pc}$ where T has been eliminated between the Wein Displacement and Stefan-Boltzmann Laws, L is the portion of IR luminosity corrected for extended star formation, λ runs from $2\ \mu\text{m}$ to the lesser of either the wavelength where the source is no longer optically thick or the peak FIR wavelength and scattering is neglected). MIR ice absorption is therefore consistent with a portion of the FIR emission being powered by the MIR rather than the optical and UV portion of the electromagnetic spectrum. However, it is necessary to be certain that the reported absorption is indeed owing to ice. As an example, Spoon et al. (2002) claim ice absorption in 18 galaxies based on $6\ \mu\text{m}$ absorption including

IRAS 17208-0014 the third brightest ULIRG. However OH bond bending needn't occur in ice alone. The absence of $3\ \mu\text{m}$ absorption in the spectra of the dust continuum dominated sources Mkn 231 and IRAS 05189-2524 presented by Spoon et al. (2002), where veiling by starlight is unimportant, suggests that an identification of water ice may be premature for these sources and refractory materials such as those studied by Greenberg et al. (1995) may provide a more convincing model. An apparent $6\ \mu\text{m}$ dip in the spectrum of Mkn 231 plotted by Weedman et al. (2005) similar in amplitude to the $6.2\ \mu\text{m}$ hump for which they report a measurement tends to confirm the Spoon et al. (2002) claim of $6\ \mu\text{m}$ absorption in this source. The spectrum of Arp 220 may be consistent with a contribution of $12.5\ \mu\text{m}$ libration mode absorption, supportive of the Spoon et al. (2002) identification of ice absorption in this source but, until recently (Imanishi et al. 2006a; Risaliti et al. 2006; Imanishi 2006), the only well confirmed case of ice absorption among ULIRGs in their sample was that of IRAS 00188-0856 where ice absorption at $3\ \mu\text{m}$ confirms the identification (Imanishi & Maloney 2003). See Imanishi et al. (2006b) for further well confirmed ice identifications.

To illustrate this we present Fig. 1 which employs a slightly detailed model to explain the absorption features observed between 2.7 and $12.4\ \mu\text{m}$. The upper panel reproduces the $3\ \mu\text{m}$ spectrum reported by Imanishi & Maloney (2003) together with an absorption model composed of amorphous ice and refractory carbonaceous absorption applied to a power-law continuum, and veiled by some starburst-like emission. The model is then applied in the lower panel with some adjustment made for expected reduced refractory absorption at longer wavelengths owing to a presumed dust temperature gradient. It has not been possible to fit the entire $3\ \mu\text{m}$ absorption without using ice. Thus, the absorption at $6\ \mu\text{m}$ also is partly attributed to water ice. With these data, $12.5\ \mu\text{m}$ water ice absorption, while included in the model, does not seem to be required so that one may conclude that two features, and particularly the degeneracy breaking short wavelength edge of the $3\ \mu\text{m}$ absorption contribute to the fairly robust identification of ice in IRAS 00188-0856. We note that the need for strong silicate absorption in this source is confirmed by the clear presence of $18\ \mu\text{m}$ silicate absorption (Imanishi et al. 2006b)

Thus, ice absorption could play a significant role in ULIRGs, but the evidence is not yet as strong as that showing that the MIR emission is often absorbed by refractory dust. Evidence for or against FIR ice emission or absorption in ULIRGs is in worse shape still. This is primarily owing to a lack of observational data. In Fig. 2 we present archival ISO LWS spectra of Mkn 231 (filled diamonds) and IRAS 17208-0014 (filled circles) which show spectral structure in the shortest wavelength detector band SW 1. This structure is compared to the spectrum of the icy source HD 161796 (Hoogzaad et al. 2002) transformed to absorption. For Mkn 231, as just noted, the absence of $3\ \mu\text{m}$ ice absorption would lead to somewhat strained geometric arguments to allow acceptance of the Spoon et al. (2002) identification of the 6

μm absorption, but once made, such arguments would likely allow absorption at even longer wavelengths. A complex geometry has already been invoked for this source on a smaller physical scale to explain its low X-ray flux (Maloney & Reynolds 2000). For IRAS 17208-0014, the present spectrum would tend to confirm the Spoon et al. (2002) identification of the $6\ \mu\text{m}$ absorption as do $3\ \mu\text{m}$ spectra (Risaliti et al. 2006; Imanishi 2006). For either source, the presence of crystalline ice implied by the possible $43\ \mu\text{m}$ absorption would imply a low cosmic ray abundance at least in the region where the absorption is produced since ion bombardment erases crystalline structure in cold ices (Moore & Hudson 1992). The inset in Fig. 2 shows the relationship between the wavelength of the $43\ \mu\text{m}$ peak and ice temperature measured by Smith et al. (1994) which we have invoked to shift the ice spectrum derived from HD 161796, an evolved ice forming star (Hoogzaad et al. 2002), beyond the corrections made for the source redshifts to better match the spectra. Inversion of these corrections would imply temperatures at which amorphous ice may exist and would be preferentially formed. Constraints on cosmic ray abundance would need account for the rate at which crystalline ice is introduced into the absorbing region either through (substantial) changes in luminosity of the source which may allow the annealing of amorphous ice to crystalline ice, processing of ice by local heat sources in the region, or the migration of crystalline ice into the region. The discovery of substantial radial molecular gas motion in the ULIRG IRAS 08572+3915 (Geballe et al. 2006) suggests the third possibility needs close scrutiny. Since the SW1 detector of LWS is problematic, these sources must be independently re-observed and the potential features confirmed before fully accepting that ice is present in these sources.

2.2. Millimeter morphology

We have examined the LWS SW1 spectra of a two other ULIRGS, Arp 220 and Mkn 273, finding no feature consistent with crystalline ice absorption. In the case of Arp 220, the FIR spectrum appears to be optically thick (González-Alfonso et al. 2004). There is every reason to think ice should be present owing to the source temperature, the clear presence of water vapor, as well as supportive MIR observations already mentioned. Here, ice may help to resolve an issue raised by Soifer et al. (1999) with regard to FIR sources that are optically thick showing any detectable emission in the MIR owing to overwhelmingly large implied MIR opacity. Since ice strongly enhances the FIR opacity compared to refractory dust, a given FIR optical depth can be achieved with less dust, up to a factor of seven in the models computed by Aannestad (1975). This effect can make the issue raised by Soifer et al. (1999) less troubling, though other approaches such as examining the effects of the dust density distribution (*e.g.* Nenkova et al. 2002) may also need to be explored as well. Ice may also have the effect of making millimeter continuum size estimates smaller than what

might be expected for refractory dust that is optically thick in the FIR since the opacity of ice mantled grains is lower than that of bare grains at millimeter wavelengths. This could yield a cuspy morphology in the millimeter where one would usually expect a relatively more flattened morphology owing to the cooler outer regions being relatively brighter in the millimeter under the assumption of higher refractory dust opacity.

2.3. FIR ice spectrum

The infrared laboratory spectrum of crystalline water ice has been well known for some time (Bertie et. al 1969) and differences between the spectrum of crystalline and amorphous ice have been exploited to aid understanding of astronomical sources (*e.g.* Dartois et al. 1998). However owing to the low thermal conductivity of amorphous ice, preparation of laboratory samples, via vapor deposition, that are thick enough to conduct investigations at wavelengths longer than 100 μm has been too difficult until recently. In particular it has been unknown whether or not amorphous ice has a feature corresponding to the broad feature centered near 150 μm identified by Bertie et. al (1969) as a phonon mode in crystalline ice. Since nature provides sources rich in amorphous ice, it may be that such a comparison could be made through observations of these sources. The spectral coverage of the ISO LWS spectrometer extended to $\sim 200 \mu\text{m}$, too short to fully cover the broad 150 μm crystalline ice feature. Comparison between the ISO LWS data presented by Dartois et al. (1998) for RAFGL 7009S, a deeply embedded ultracompact H II region, and the submillimeter observations provided by McCutcheon et al. (1995) yield a modified optically thin blackbody parameter set of $T=27 \text{ K}$, $\beta=2.1$ (where the dust emissivity is proportional to $\lambda^{-\beta}$) when attempting to match data near 190 μm . The large value of β is suggestive of the presence of a feature similar to that of crystalline ice in this amorphous ice dominated source. However, full spectroscopic confirmation is needed to decide if the long wavelength departure of the data from the model of Dartois et al. (1998) indicates the existence of an amorphous ice feature analogous to the 150 μm crystalline ice feature.

Laboratory work by Curtis et al. (2005) has explored the optical properties of amorphous ice between 15 and 200 μm . There is little question that most of the ice in the thick films used by Curtis et al. (2005) deposited at $T \leq 126 \text{ K}$ differs from ice deposited above this temperature since the wing of the libration band is clearly shifted so it seems safe to conclude that amorphous ice, clearly present in the thinner samples, is also largely present in the thicker samples despite issues related to the low thermal conductivity of amorphous ice which hampers the (rapid) growth of thick samples. Gerakines et al. (2005) have also had recent success in growing thick samples of amorphous ice using low deposition rates.

Schober et al. (2000) take a different approach: annealing samples of high density amorphous ice into the low density amorphous ice found in space. As with the LWS spectroscopy, the new amorphous ice optical constants (Curtis et al. 2005) do not extend to the wavelength regime ($300\ \mu\text{m}$) where crystalline ice shows absorption whose wavelength dependence is described by λ^{-4} (Bertie et al. 1969). Unlike natural sources, however, where temperature and grain size effects make full spectral coverage of a broad feature nearly absolutely necessary to ascertain its reality, the controlled laboratory conditions allow a reasonable extrapolation to be considered reliable. The finding of Curtis et al. (2005) that the imaginary part of the refractive indices of amorphous and crystalline ice are very similar between 100 and $200\ \mu\text{m}$ would appear to be consistent with the suggestion of Schober et al. (2000) that the order in amorphous ice indicated by sharp features in inelastic X-ray scattering data may be owing to a hydrogen network that is also present in crystalline ice. If this order is indeed present, then a shared spectral structure for the interaction of (FIR) photons with phonons between the two types would allow a first order substitution of crystalline ice optical constants for the unknown values for amorphous ice beyond $200\ \mu\text{m}$.

2.4. FIR ice emission

Turning to photometry, and returning to ULIRGs, if we accept the Spoon et al. (2002) classification scheme then the spectrum of IRAS 14348-1447 as reported by Genzel et al. (1998) or Charmandaris et al. (2002) must be considered Class II, that is $6\ \mu\text{m}$ “ice” absorption is present and partially filled in by $6.2\ \mu\text{m}$ polycyclic aromatic hydrocarbon emission. This source occupies an extreme position in the dust emissivity (β) vs. $100\ \mu\text{m}$ optical depth (τ_{100}) diagram given by Klaas et al. (2001) with both high τ_{100} (5) and β (2). Since the effects of optical depth and emissivity are intertwined, a lower optical depth can imply a larger value of β . For example, $\beta = 2.4$ and $\tau_{100} = 0.1$ does about as well as the Klaas et al. (2001) parameters for data longward of $100\ \mu\text{m}$. However, values of β larger than 2 are not generally found except where ice is thought to be present (*e.g.* Lis et al. 1998) or dust temperatures are lower than found in ULIRGs (67 K for the Klaas et al. (2001) fit or 26 K at the lower optical depth and larger β tested here). In Fig. 3 we compare the fit proposed for IRAS 14348-1447 by Klaas et al. (2001) with an alternative model. The model shown by the dashed line is that of Klaas et al. (2001), while that shown by the thick solid line is a core-mantle grain model taken from Aannestad (1975) but modified to have amorphous ice features in the following way: First, opacity data from Smith et al. (1994) for crystalline ice cooled to 70 K was matched to the Aannestad (1975) curve for $V_m/V_c=0.95$ by inducing a ν^{-1} dependence to approximate the Mie calculation results along with the addition of an underlying continuum opacity. Second, amorphous ice opacity data (Smith et al. 1994;

deposited at 10 K and warmed to 70 K) was substituted between 30 and 70 μm based on this matching after adjustment for the differing sample thicknesses. This opacity curve was used to calculate a model with 16 and 71 K components. If we take temperature and optical depth as free parameters for the Klaas et al. (2001) fit (2 parameters; normalization fixed by IRAS) and two temperatures, two optical depths, and the relative contribution at 90 μm of these two components as 5 free parameters for the present model then we may estimate how well the two models represent the data if we know something about the errors in the data. The statistical errors for the data are thought to be small but the absolute calibration error could be large, $\sim 30\%$. What is important for comparing models is the relative accuracy from filter to filter. We have thus assumed 13% errors for the ISOPHOT data to give a filter-to-filter accuracy of 20% (Klaas et al. 2000). The fit of Klaas et al. (2001) for data longward of 20 μm is unacceptable ($P(\chi^2, \nu)=0.02$) under our assumption about the errors. A marginally acceptable fit ($P(\chi^2, \nu)=0.4$) is found for the amorphous ice model. Detailed inspection of the ice fit suggests that the 150 μm ice feature is not accounting for all of structure in the data. The thin solid line ($V_m/V_c=0.33$, $T=28.8$ K; $\tau_{90} = 0.2$ and $V_m/V_c=0.95$, $T=80.5$ K, $\tau_{90} = 0.08$ crystalline ice; onion-skin model with warm, $T=180$ K, refractory dust in the interior) shows that this might be possible. However, our method of substituting amorphous for crystalline ice is unlikely to work well for the thin mantle used here. Given the assumption regarding the data errors made here, it is not possible to make a clear claim that ice emission is detected in this source. Assuming larger errors could make both low free parameter models acceptable while reducing the errors could make the simpler ice model unacceptable while the more complex model cannot be evaluated via reduced χ^2 . Clearly, *Spitzer* MIPS SED mode observations could be definitive since the strong 70 μm curvature in the ice models cannot be produced with standard refractory dust.

Thus, both astronomical and laboratory far infrared data leave questions about ice unanswered. Crystalline ice has a feature near 150 μm which has yet to be completely compared with amorphous ice. Comparison between crystalline and amorphous ice has been made near 40 and 60 μm and they are quite distinct whereas they are similar between 100 and 200 μm . Beyond 200 μm questions remain which are presently answered by extrapolation of the laboratory data and hints from the astronomical data. Substituting crystalline ice for more common (in space) amorphous ice to consider wavelengths longer than 100 μm could add to (systematic) uncertainties in photometric redshift estimation that can not be well addressed without further observations or measurements. Regardless of the remaining issues concerning the 150 μm feature, for the main purpose of this work it is prudent to consider the more extreme consequences of crystalline ice emission on redshift estimation which are examined after the next section.

3. Ice at high redshift

3.1. Pair instability SNe enrichment

Just as interplanetary grains may preserve a record of the sources of ISM enrichment occurring at what is presently observed to be $z = 0.43$, the solid phase of the ISM at high redshift may also record the conditions of the earliest enrichment. Particularly for sources that contribute to the reionization of the universe ($7 < z < 14$; Spergel et al. 2006), scenarios which attribute substantial enrichment to pair instability SNe early on may leave a mark on the solid phase of the ISM which could linger through some subsequent processing. A chief attribute of pair instability SN enrichment is an early high abundance of oxygen relative to other metals that usually deplete to the the solid phase of the ISM.

For example, a $186 M_{\odot}$ progenitor yields number abundance ratios of O:Si:C:S:Mg: ^{56}Ni = 126:29:15:10:8:1 (Heger & Woosley 2002) which, after formation of CO (29 O removed), olivine (16 O and 4 Si removed), silica (50 O removed), and SO_2 (20 O removed), leaves 9% of the oxygen available to form OH and H_2O . For a $100 M_{\odot}$ progenitor, O:C:Mg=48:9:1 with little Si, S or ^{56}Ni leaving 80% of the oxygen available to combine with hydrogen assuming the refractory solid state is MgO. In the absence of ^{56}Ni , the formation of solids should be enhanced since it may commence at a higher density in the SNR. These estimates for the available oxygen are essentially lower limits, more complete treatments which consider the possibility that the ejecta are unmixed (Nozawa et al. 2003; Schneider et al. 2004; allowing the formation of graphite for example) would leave an even larger fraction of oxygen available. Thus, we might expect grains with large mantle-to-core volume ratios to result from a period of pair instability SN enrichment. The continued presence of these ice grains would depend on the rate of reprocessing of this initial solid phase in the ISM.

3.2. Ice emission in a high redshift quasar

The Gunn-Peterson trough in QSO J1148+5251 ($z = 6.42$; Bertoldi et al. 2003b) suggests that this source may be participating in the last phases of reionization (Fan et al. 2003). That the quasar exists indicates that the source has been contributing to reionization for some time and we may take the beginning of reionization as an estimate of it's age (~ 500 Myr) which gives a high average accretion rate for a blackhole mass of $3 \times 10^9 M_{\odot}$ (Willot et al. 2003). Thus, it seems plausible that pair instability SN enriched material with a high ice content is being supplied toward the center of this activity as the blackhole and presumably its stellar system grow in mass. On the other hand, ice also forms in the more evolved ISM of the Galaxy so an indication of the presence of ice needn't be fully attributed

to ice rich regions that might be formed by pair instability SNe.

Fig. 4 shows an indication that the rest frame FIR emission from QSO J1148+5251 is better explained by ice than refractory dust emission. Three models are compared to photometric observations: 1) a refractory model (dashed line $T=55$ K; $\tau_{60} = 0.3$; $\beta = 2$) is similar to that given by Beelen et al. (2006), 2) a simple ice model (dot-dashed line; $T=43$ K; $\tau_{60} = 0.4$, $V_m/V_c=5.6$ amorphous), and 3) a more complex ice model described below (solid line).

In Fig. 4, it is not possible to formally access the goodness of fit through a reduced χ^2_ν calculation even for the refractory dust model (dashed line) since the number of free parameters (normalization, temperature, optical depth, and opacity index) is the same as the number of points to be fit. If one were to assume $\beta = 2$ owing to insufficient time since the first enrichment to produce large grains then $\chi^2_\nu = 10.7$ which strongly rules out ($P(\chi, \nu)=0.001$) this model. That the fit is done by eye probably does not affect this assessment but a failure to account for systematic errors could since different groups give $850 \mu\text{m}$ photometric estimates using the same data that vary by as much as the refractory dust model differs from the present data. By selecting a particular mantle-to-core volume ratio (5.6) we may comparably provide a single degree of freedom and obtain $\chi^2_\nu = 3.9$ (dot-dashed line) which would indicate that the model is not fully ruled out by the data ($P(\chi, \nu)=0.05$) and is an improvement on the refractory dust model, again with the proviso that we have only considered statistical errors. More elaborate (multi-temperature) refractory dust or ice mantled grain models can fit the detections essentially perfectly and are useful to calculate as they can indicate what further observations would be decisive. The solid line in Fig. 4 is such a model where $T=71$ K; $\tau_{60} = 0.4$ ice-mantled dust is obscured by $T=24$ K; $\tau_{60} = 0.4$ ice-mantled dust. A similar model using $\beta = 2$ refractory dust (not plotted; $T=300$ K; $\tau_{60} = 0.1$ is obscured by $T=18$ K; $\tau_{60} = 1$ dust) exceeds the plotted $400 \mu\text{m}$ upper limit (arrow in Fig. 4; $0.39 \text{ mJy } 3\sigma$; Bertoldi et al. 2003a) by a factor of 1.9 and is unphysical in a number of ways including that the cool component is cooler than the CMB at $z = 6.42$. The ice models distinguish themselves from the plotted refractory dust model by being fainter by at least a factor of 4 at rest wavelength $400 \mu\text{m}$ (3 mm observed frame). The present upper limit does not distinguish these cases. Such a measurement should be possible using CARMA. Determining the composition of the emitting material can also affect estimates of the dust mass and thus estimates of the amount of past enrichment (and star formation) in the QSO J1148+5251 system. For the present ice model, 7 times as much refractory dust would be needed to produce the same FIR opacity so that a lower level of total enrichment might be accommodated.

Finally, at high redshift, where theory suggests that we might most anticipate it owing

to expectations about early ISM enrichment, we find evidence for FIR ice emission which, while still debatable, seems moderately persuasive and which can be relatively easily checked with further observations using existing telescopes. Now we may turn to our main theme. We have employed amorphous ice to consider IRAS 14348-1447 and QSO J1148+5251, but now we consider crystalline ice both because its effect on redshift estimation is the most dramatic and because ice may form at fairly warm temperatures in the SNRs associated with pair instability SNe.

3.3. Ice emission in 450 μm submillimeter sources

A set of sources that could be at high redshift and which demonstrate the effects of ice are reported by Pope et al. (2005). They are detected at 450 μm but not at 850 μm . We consider the 7 sources tabulated by Pope et al. (2005) and two sources from the original list of Borys et al. (2003) which were recovered above 3.5σ by Pope et al. (2005). These have drawn our attention because the reported 850 μm upper limits indicate large values of β (Borys et al. 2004; based on original list). Large values of β can indicate the presence of ice emission. If we generate 3σ lower limits to the 450-to-850 μm flux density ratios using the 450 μm measurements less $3/\sqrt{2} \times \sigma_{450}$ together with $3/\sqrt{2} \times \sigma_{850}$ 850 μm upper limits then the lowest lower limit is 8.7 and is only one of two that can be consistent with $\beta < 2$ dust. This method of calculating limits can be more conservative than calculating the ratio of the 450 measurement to the 850 μm 3σ upper limit (giving 13.4 in this case) but its extension to 2σ should be viewed with caution since detections at the 2.9σ level are customarily reported as 3σ limits. In such situations, when data with comparable signal-to-noise ratios become available, the “ 2σ extension” may be violated much more frequently than the name implies if many of these near misses lurk in the original data. However, Pope et al. (2005) report no detection from applying the method of Caillault & Helfand (1985) (stacking) to the 850 μm data at the positions of the 450 μm sources they detect above 3.5σ . In five cases where upper limits are calculated below we substitute the ratio of the 450 μm 3σ upper limit-to-the 850 measurement when it gives a more conservative value.

In Fig. 5 we plot, as a function of redshift, the 450-to-850 μm flux density ratio calculated for a series of SEDs. The dashed line is for a model with $T=60\text{ K}$, $\beta=2$, and $\tau_{90}=2$. On this line are plotted at $z = 0.9$ and $z = 0.5$ the 3σ lower limits (filled circle and diamond) for SMM J123603+620942 and J123631+620657. The arrows in the figure extend to the 2σ lower limits. In these cases the argument given by Borys et al. (2003) for $z < 1$ may be applied directly, though tenuously, at the 3σ level with no assumptions about ice but this is not the case for the 7 remaining lower limits. There may be some difficulty however

accommodating these two sources at these low redshifts unless sources with 0.2–2 Jy level flux densities are present at 70 μm while Frayer et al. (2006) find about four ~ 30 mJy sources at 70 μm in this region and we are unaware of any IRAS sources in this field. At these low redshifts, it is a losing proposition to attempt to increase the dust temperature to increase the redshift to avoid the 70 μm constraint in an effort to avoid requiring ice emission. When ice is invoked, then these and the remaining lower limits may all be accommodated but the range of consistent redshifts expands. The remaining curves in Fig. 5 correspond to increasing ice temperature. The dot-dashed curve uses an SED similar to that shown in Fig. 1 ($T=30$ K), the triple-dot-dashed curve has $T=50$ K as in Fig. 7., and the solid curve has $T=150$ K; $\tau_{90} = 0.04$ and $V_m/V_c=5.6$ for all ice models. For the solid curve, ambiguity between amorphous and crystalline ice is physically resolved in favor of crystalline ice. The SMM J123603+620942 and J123631+620657 limits are replotted on the solid curve giving a redshift limit $z < 10.2$. This limit is little changed if the maximum possible ice temperature (170 K) is used. All the 3σ limits can be accommodated at $z = 9.5$ but only SMM J123603+620942 and J123631+620657 can also be accommodated there at the 2σ level. SMM J123657+622033 (filled square) shows this clearly where it is plotted at $z = 9.6$. The 2σ level for SMM J133747+621600 (filled clover leaf) also constrains the ice temperature to be $T \gtrsim 40$ K. It is plotted on the $T=30$ K curve at $z = 1.9$. The remaining sources other than SMM J123727+621042 are plotted with redshift upper limits well within the epoch of reionization. However, as with sources plotted on the $T = 30$ K curve, the 2σ limits cannot be accommodated for $z \gtrsim 2.5$. That 7 of 9 of the 450 μm sources in the GOODS-N field require ice to explain the 850 μm non-detections without recourse to any other constraint suggests strongly that the possible effects of ice emission must be considered when interpreting submillimeter observations. Ice dramatically changes redshift limits: by a factor of 20 for SMM 123631+620657.

From the other direction, for the sources with 850 μm detections and 450 μm upper limits that also have estimated redshifts (Borys et al. 2004) we may also begin to constrain the presence of ice. 14 upper limits are plotted in Fig. 5 as open circles for sources where a redshift estimate is given. The open diamonds are also upper limits plotted (but without arrows to avoid crowding) at the lower limits to their redshift given by Borys et al. (2004). For redshift estimates with $z < 3$ the upper limits are constraining on the likelihood that optically thin ice contributes to the FIR opacity: at the 2σ level (arrow heads) little $T > 30$ K optically thin ice seems to be needed. At the 3σ level 4 of 11 sources could be consistent with a contribution of optically thin ice emission to the source SEDs. One source with a redshift lower limit ($z > 2.7$; SMM J123652+621225) needs to be optically thick and cool ($T \sim 40$ K) or at a higher redshift as already noted by Borys et al. (2004). The remaining sources with with redshift estimates above 3 or redshift lower limits are not constraining

on the presence of ice. The present considerations suggest that the 450 and ($z < 3$) 850 μm detected sources differ physically in that the former have optically thin ice emission that dominates their FIR opacity while the latter may be optically thick at $850/(1+z)$ μm or that refractory dust dominates their FIR opacity or both. The average 450-to-850 μm ratio for the 850 μm source calculated from the stacked 450 μm and the average of the 850 μm flux densities reported by Pope et al. (2005) is 0.5 which we have plotted as a small open square at $z = 4.25$. The plotted redshift would be consistent with $T=30$ optically thick material or $T=20$ optically thin ice or $\beta = 2$ dust. If it is true that 850 μm sources are on average fainter at 450 μm than at 850 μm then it seems at though many of the 850 μm sources must lie at $z > 4$ and ice may be needed to make them detectable at 850 μm with ULIRG luminosities (see end of Sec. 4.2). We do worry, however, that the stacked 450 μm flux is underestimated owing to the smaller 450 μm beam or that the data were normalized prior to stacking making the reported units ambiguous. QSO J1148-5251 is also plotted (small filled circle). As discussed above, it seems to require ice emission.

Just as detected 850 μm sources must be at least ultraluminous, so also must the detected 450 μm sources be hyperluminous ($L > 10^{13} L_{\odot}$). In Fig. 6 we plot the models shown in Fig. 5 giving their 450 μm brightness as a function of redshift under the following assumptions about luminosity: The models for refractory dust, and ice at $T=30$ and 50 K are ten times more luminous than ULIRG IRAS 00188-0856 (Fig. 1), the model for $T=150$ K ice is 10 times more luminous still, and we have also plotted the complex amorphous ice model for QSO J1148+5251 at it's observed luminosity (short dashed line and filled circle; $\sim 10^{13} L_{\odot}$; Beelen et al. 2006). The brightnesses of the 450 μm sources given by Pope et al. (2005) lie in the range 77-to-291 mJy so that the plotted models would need to be scaled up by a factor of a few to cover this range fully unless the sources are at $z < 0.2$. For example, one of the brighter sources (SMM J123631+620657; 263 mJy) would have a luminosity of $6 \times 10^{14} L_{\odot}$ for the $T = 150$ K ice model if located at $z = 9.5$, a factor of three higher than the most luminous hyperluminous source listed by Verma et al. (2002). It's luminosity would be 10 times lower for the $T = 30$ K ice model located at $z = 2$, near the middle of the distribution of luminosities in their list. From Fig. 5 we estimate that the 450 μm sources would populate the redshift ranges 1–3 and 5–10, with the latter range having a larger comoving volume by a factor of 1.7. If ice is only important close to reionization so that the sources were all at $9.2 < z < 10.2$ (see solid line in Fig. 6) then the luminosities require about a tenth of the stellar mass of M87 per source to be involved in star formation. The space density would be $2.5 \times 10^{-5} \text{ Mpc}^{-3}$, comparable to the local density of clusters of galaxies (Bahcall et al. 2003) and the luminosity density would be $\sim 5 \times 10^9 L_{\odot}/\text{Mpc}^3$ (comoving), about a factor of 100 higher than the local FIR value (Saunders et al. 1990). This would then imply a minimum of 10^3 recombinations per proton if the 450 μm luminosity traces a factor of ten smaller

ionizing luminosity: about 10^2 more recombinations than for the lifetime of a typical H II region which seems too high for reionization unless dust competes efficiently for reionizing photons.

On the other hand, there are six $850\ \mu\text{m}$ sources with flux densities above 20 mJy listed by Pope et al. (2005) which could be close to hyperluminous (see Fig. 7) so that we need only postulate a similar population which is (thus far) invisible a $850\ \mu\text{m}$ owing to the effects of ice and thus expect to find these sources at a range of redshifts.

There is very clear evidence of ice rather than dust providing the FIR opacity in 7 of the 9 $450\ \mu\text{m}$ sources considered here. But, the redshifts may or may not be high and additional photometry is needed to constrain the redshifts.

4. HDF 850.1 and ice

4.1. $z = 5$

The search for counterparts at other wavelengths to the brightest $850\ \mu\text{m}$ source in the Hubble Deep Field has been arduous but Dunlop et al. (2004) make a convincing case for detections in the radio and near infrared (NIR) and summarize submillimeter observations. Modeling (Aretxaga et al. 2003) of these observations leads them to conclude that the redshift of HDF 850.1 lies in the range 4.1 ± 0.5 . Since the SED of a high q ULIRG (IRAS 08572+3915) is included in the 20 templates in the model input, the effects of the change in the radio-FIR relation for ULIRGs compared to lower luminosity galaxies noted in the introduction should be partly represented in their estimate. Similarly, the suggestion of ice emission in the SED of IRAS 14348-1447 (Fig. 3) could also influence the estimate if the photometric data were used directly rather than fitted with a modified blackbody. In general, reliance on modified blackbodies will give lower estimated redshifts for cooler sources when more than one point on the Rayleigh-Jeans curve is available, as is the case for HDF 850.1, but the addition of an ice emission feature can increase the estimated redshift even for a cool source.

As one example, the bow-tie shown in Fig. 1 on the FIR continuum corresponds to the range of redshift one would calculate for HDF 850.1 based on two estimates of its $850\ \mu\text{m}$ flux density (Dunlop et al. 2004; Wang et al. 2004) and the 1.3 mm flux density reported by Downes et al. (1999). That is $5.4 < z < 5.6$. It should be noted, even before describing the model upon which this is based, that a detailed comparison between the SED shown in Fig. 1 and the optical and NIR limits and detections for HDF 850.1 is not possible owing to insufficient wavelength coverage for IRAS 00188-0856. See Dunlop et al. (2004) fig. 6 for

a comparison with data from two ULIRGs and a luminous infrared galaxy calculated for a range of redshifts. However, the effects of far infrared ice emission can be demonstrated with this example. The model, the short-dashed line in the lower panel of Fig. 1, is based on curves given by Aannestad (1975) which are the results of calculations of the optical properties of ice mantled crystalline silicate grains. And, it is crystalline water ice in the mantles. We chose the mantle-to-core volume ratio = 5.6 curve to most closely match the ratio of 3 μm ice to silicate optical depth used in the model shown by the solid lines in Fig. 1. For a number of reasons this choice is probably not fully constrained by this ratio: the optical depth to which the silicate absorption is sensitive may be larger than for ice; an odd shift in the wavelength of the silicate feature may indicate a pyroxene composition with a different feature-to-continuum optical depth ratio than usual; the crystalline silicate in the Aannestad (1975) calculation is somewhat dissimilar to astrophysical silicate models. However the first two effects may be compensating so that as a rough abundance analysis, the expectation that ice would dominate the FIR opacity in this source seems well founded. This condition, and the need for the ice emission to be moderately optically thin are really the only two requirements for ice to strongly affect redshift estimation. The optical depth of the model of far infrared emission shown in the lower panel of Fig. 1 is set to correspond to the 3 μm ice optical depth used in models shown by the solid line in the upper panel (where ice and refractory material contribute equally to the absorption optical depth at 3.1 μm). The temperature of the far infrared emission model is set to roughly reproduce the IRAS 60 and 100 μm measurements. This temperature also accentuates the effects of the broad 150 μm feature over which the HDF 850.1 data are displayed. The range of redshifts needed to place HDF 850.1 on this model falls outside of the range estimated by Dunlop et al. (2004) and gives a first indication that the effects of ice on photometric redshift estimation (as opposed to just limits) can be significant.

4.2. $z = 13$

As noted in the introduction, using local ULIRGs to understand submillimeter sources is a sensible approach if their properties are not strongly affected by cosmic evolution. However, at higher redshift, this proviso seems fairly likely to break down. Many local ULIRGs appear to be produced in the mergers of gas rich spiral galaxies and it has been argued (Mihos & Hernquist 1996) that the dynamical stability provided by bulges may preserve gas reservoirs for the final merger stages associated with some ULIRGs. Owing to the finite lifetime of the universe, there are earlier periods when the precursor systems may not resemble present day precursors in their dynamical state or star-to-gas mass ratio. It is not at all clear that seed SMBHs (Osterbrock 1993) would be present at sufficient mass to

allow accretion to be an energetically important or dominant power source as suspected for local ULIRGs (*e.g.* Imanishi et al. 2006a). Thus, in what follows we assume star formation as the main power source at higher redshift. A sketch of how crystalline ice might exist in a primordial galaxy environment is also given to explore the plausibility of a very large effect of ice on redshift estimation. It is to be noted that giving up a central power source such as would be provided by an AGN would usually mean that ice mantled grains would contribute little to the FIR emission since most of the energy that powers FIR emission would be absorbed in reactive photodissociation regions (PDRs) rather than in molecular clouds where ice is thought to exist unless an improbable scenario involving an overabundance of protostars such as that proposed by Roussel et al. (2003) but previously discounted by Dudley & Wynn-Williams (1997) is invoked. Below we argue for such an overabundance.

In Fig. 7 we show the observations of HDF 850.1 at $z = 12.6$. This is 18 confidence intervals beyond the Dunlop et al. (2004) estimate. So far as we can tell, neither the new Z band upper limit reported here, nor the released *Spitzer* IRAC and MIPS GOODS images (Dickinson et al. 2006) rule out either the model shown in Fig. 7 or the analysis of Dunlop et al. (2004) so long as a reddish ULIRG (see Dudley (1999) for a discussion of 12-to-60 μm flux density ratios in ULIRGs) is used as a basis for the Dunlop et al. (2004) analysis. Dunlop et al. (2004) argue that the lensing source (solid diamonds in Fig. 7) is evolved, in which case much of the tentative observed frame 24 μm flux density could be owing to HDF 850.1 but little of the 8 μm flux density. At $z = 4.1$, Mkn 231 and 273 could be too blue to account for this level of emission whereas Arp 220 or IRAS 17208-0014 would not violate this datum if treated as an upper limit. On the other hand, at $z = 1.1$ the chances of finding a younger elliptical galaxy to act as a lens are increased so that some or all of the observed 24 μm flux density could be owing to the lensing galaxy. This would still not rule out the Dunlop et al. (2004) redshift estimate for HDF 850.1 but would accommodate the present estimate under the assumption of the plotted starburst model. The shaded region in Fig. 7 shows a possible range for the spectral shape of the lens source emission. The source labeled 1b in fig. 8 of Wang et al. (2004) may also contribute to the 24 μm emission though only slightly to the IRAC data. If it is similar to NGC 253, and at a redshift of $z_{\text{ph}} = 1.76$ (Fernández-Soto et al. 1999) then up to $\sim 30\%$ of the 24 μm flux density might be attributed to this source but again negligibly at 850 μm .

The model for HDF 850.1 shown in Fig. 7 (thick gray line) is similar to that shown in Fig. 1 in that it has the same mantle-to-core volume ratio and optical depth however the temperature is higher as it must be owing to the higher CMB temperature at $z = 12.6$. Whereas in Fig. 1, the 150 μm ice feature spectral structure influences the redshift placement of the HDF 850.1 data, in Fig. 7, shorter wavelength spectral structure also owing to ice is influential. Interestingly, assuming that there is a foreground neutral intergalactic medium

as a result of incomplete reionization (Spergel et al. 2006), one would expect Gunn-Peterson saturation or a Ly α blackout to occur in the H band for $z = 12.6$ the shortest wavelength band for which HDF 850.1 is detected. This is represented by the change from black to gray in the thin line using a Heaviside function as multiplier. Here the thin line is a young starburst spectrum generated using Starburst99 (Leitherer et al. 1999). It is notable that taking the onset in redshift of the Gunn-Peterson trough to be ~ 6 (Fan et al. 2004) absorption at the Lyman limit at $z < 12.6$ easily overlaps Ly α absorption between $z = 6$ and $z = 9.2$. One expects pretty thorough opacity shortward of Ly α .

While the choices of parameters of the starburst model are meant only to be suggestive, for the model shown in Fig. 7, the free-free emission expected based on the rate of production of ionizing photons would explain about 20% of the observed radio emission (following Scoville et al. 1991) while retaining the starburst model as it is and correcting for sufficient extinction to account for the model infrared emission would over produce the radio emission so that a lower contribution of stars which produce ionizing photons to the observed frame K' band flux might provide a more likely scenario. Alternatively, invoking a chemical trigger for star formation discussed below, it is conceivable that an object could be caught in a phase when a sufficient number of stars are in an ultracompact H II region configuration that, given a sufficiently high ionization parameter, higher than usually required if the gas-to-dust mass ratio is high owing to low enrichment, free-free emission would be suppressed (*e.g.* Bottorff et al. 1998).

As noted in the introduction, sources at high redshift should eventually drop out of 850 μm surveys. In Fig. 8 we plot, for the same far infrared luminosity, the expected 850 μm brightness as a function of redshift for an Arp 220-like SED and the two distributions shown in Figs. 1 and 7. The 30 K model is truncated at $z = 11$ since the cosmic background radiation temperature exceeds the model temperature above this redshift. As can be seen, the models with ice select for high redshift sources assuming such sources exist. For the 30 K model the brightest (non-local) source would be found near a redshift of 5 and for the 50 K model near a redshift of 13. Should ice play the role proposed here in a moderate fraction of the detected 850 μm sources, it would be of little surprise that the brightest source in the HDF (850.1) would be among them.

4.3. Why star formation?

Our choice of presenting a model that uses star formation as a power source may seem strange given that PDRs would be inefficient at producing ice emission which we require to allow, for example, HDF 850.1 to be detected at $z = 13$. One phase of star formation that

does allow MIR radiation to heat ice is the protostar phase. This phase is brief compared to O star life times and thus would not typically be expected to provide the dominant source of FIR radiation in a galaxy. Protogalaxies, however, are by definition required to be young, so that while the argument concerning the relative brevity of the protostar phase cannot be ignored, it may be overcome if the star formation rate is increasing rapidly with time. And, it is just such sources that one might expect to be observed as they populate the top of the infrared luminosity function since they would be the most efficient at converting radiation to FIR wavelengths.

A rapidly increasing star formation rate might be expected in a situation where the gas cooling efficiency is increasing owing to ongoing initial enrichment. A positive feedback can lead to an exponentially increasing system response. The number at the right hand of Fig. 8 shows the 850 brightness (in mJy) of the three SED shapes considered here if we adopt the lensing amplification proposed by Dunlop et al. (2004) for HDF 850.1 for a source with the FIR luminosity of IRAS 00188-0856. The increase in luminosity required to match the Hughes et al. (1998) estimate for HDF 850.1 would be a factor of 2.3 for the dashed curve taken at a redshift of 13. This would then correspond to $\sim 4 \times 10^{12} L_{\odot}$ (*e.g.* Fig. 7) or 10^7 O stars and 1.5×10^{11} G0 stars for a Salpeter initial mass function ($m^{-2.35}$), or roughly a galaxy's worth of star formation. This then would be the limit for the continued exponential increase in the star formation rate: the amount of available enrichable gas. Night et al. (2005) find 4 objects with $10^{11} M_{\odot}$ in stars at $z = 6$ in their largest cosmological simulation (142 Mpc; large enough to contain ~ 1 ULIRG at $z = 0$). Thus, there is some suggestion that relatively massive objects (or perhaps regions that will become objects) are forming their stars a few dynamical timescales earlier than this. Notwithstanding the existence of QSO J1148+5251 and other high redshift quasars, it seems to us that there is a need to account for massive sources at intermediate redshift which last formed stars near $z = 13$ (Stockton et al. 2004; Jimenez 2000) as well as the apparent monotonic increase in the comoving rate of gamma-ray bursts out to $z = 7$ (Le & Dermer 2007).

However, in the low-to-moderate redshift universe, we would usually take ice emission as an indication of a buried compact power source at least at ULIRG luminosities, and, should blackhole growth commonly reach $\sim 10^7 M_{\odot}$ by $z = 13$, as must happen at least occasionally given the existence of QSO J1148+5251, then our low-to-moderate redshift explanation could also apply during reionization.

5. Summary and prospects

Far infrared ice emission may be crucially important to understanding the far infrared emission of sources at high redshift and may strongly affect the range of redshifts estimated for submillimeter sources, even placing them at reionization redshifts. Observations of infrared ice emission are definitive in Galactic protostars and the winds of evolved stars but are scant and not fully persuasive for the local analogs of the submillimeter sources, the ULIRGs. This, despite mounting evidence that ice is involved in absorbing much of the energy that is finally emitted in the far infrared in a substantial fraction of ULIRGs.

We find stronger indications that ice emission is important at high redshift. The data for QSO J1148+5251 as well as the 450 μm sources cataloged by Pope et al. (2005) are both strongly suggestive. We feel that further investigation along these lines could be quite fruitful.

We’ve considered two models where the presence of far-infrared emission features owing to ice in the SED of HDF 850.1 would place it at redshifts larger than the range estimated without ice by Dunlop et al. (2004). In the first, the use of crystalline ice at 150 μm as a substitute for amorphous ice is probably justified, subject to further laboratory investigations of amorphous ice. In the second, consideration of a first chemical enrichment mechanism suggests that crystalline ice could be present at early times while energetic and timescale considerations may be compatible with protostars in protogalaxies producing the sort of features we consider here. In the second model, a Lyman α blackout would be consistent with the NIR photometry for HDF 850.1. However, we do not prefer this model and its higher redshift over the redshift range estimated by Dunlop et al. (2004) or $z \sim 5.5$ from our first model. What we find to be important is that far infrared ice emission could have such a dramatic effect on the estimated redshift. It should be noted that redshifts estimated from the radio-FIR relation could also turn out to be lower when ice emission is invoked since a large submillimeter-to-radio flux density ratio is easier to produce with high β at some redshifts. So, the main conclusion of this work is that ice broadens the range of redshifts to be considered for a given submillimeter source and that ice is quite likely to be important at high redshift.

Some astronomical observations which could aid progress on open issues are:

- Continuum observations at 3 mm of QSO J1148+5251 may confirm ice emission in this source.
- The Atacama Large Millimeter Array may be able to isolate the transition from dust to free-free/synchrotron emission for sources of this type and allow more reliable redshift

estimates.

- Investigating the role of ice emission locally could be taken up using SOFIA or Spitzer.
- Very low resolution H-band spectroscopy might test the possibility of a Lyman α blackout for HDF 850.1.
- Molecular studies which target H₂O and OH maser emission may give definite redshifts using a new generation of radio telescope arrays even if the continuum is below detection limits.

Colleagues have commented helpfully at various stages of this work. Some are: S. Chubb, E. Dwek, J. Fischer, P. Gerakines, A. Li, M. Moore, L. J. Rickard, E. Shettle, and H. Smith and an anonymous referee. Research in infrared astronomy and particularly the astrophysics of celestial backgrounds at the Naval Research Laboratory is supported by the Office of Naval Research (USA). This publication makes use of data products from the Two Micron All Sky Survey, which is a joint project of the University of Massachusetts and the Infrared Processing and Analysis Center/California Institute of Technology, funded by the National Aeronautics and Space Administration and the National Science Foundation. Use is also made of the USNOFS Image and Catalog Archive operated by the United States Naval Observatory, the archive of results from the ESA sponsored *Infrared Space Observatory* mission, the NASA/IPAC Extragalactic Database operated by JPL and Caltech, and data from the GOODS project from NASA’s *Spitzer* and *Hubble Space Telescopes*.

REFERENCES

- Aannestad, P. A. 1975, ApJ, 200, 30
- Aretxaga I., Hughes D. H., Chapin E. L., Gaztanaga E., Dunlop J. S., 2003, MNRAS, 342, 759
- Athey, A., Bregman, J., Bregman, J., Temi, P., 2002, ApJ, 571, 272
- Bahcall, N., et al., 2003, ApJS, 148, 243
- Beelen, A., Cox, P., Benford, D. J., Dowell, C. D., Kovács, A., Bertoldi, F., Omont, A., Carilli, C. L., 2006, ApJ, 642, 694
- Bertie, J. E., Labbé, H. J. & Whalley, E. 1969, J Chem Phys, 50, 4501
- Bertoldi, F. et al. 2003, A&A, 409, L47

- Bertoldi, F., Carilli, C. L., Cox, P., Fan, X., Strauss, M. A., Beelen, A., Omont, A., Zylka, R., 2003, A&A, 406, L55
- Borys, C., Chapman, S., Halpern, M., Scott, D., 2003, MNRAS, 344, 385
- Borys, C., Scott, D., Chapman, S., Halpern, M., Nandra, K., Pope, A., 2004, MNRAS, 355, 485
- Bottorff, M., Lamothe, J. Momjian, E. Verner, E. Vinković, D. & Ferland, G. 1998, PASP, 110, 1040
- Brinchmann, J. et al. 1998, ApJ, 499, 112
- Caillault, J.-P., Helfand, D. J., 1985, ApJ, 289, 279
- Charmandaris, V. et al. 2002, A&A, 391, 429
- Condon J. J., Huang Z.-P., Yin Q. F., Thuan, T. X., 1991, ApJ, 378, 65
- Curtis, D. B., Rajaram, B., Toon, O. B., Tolbert, M. A., 2005, Applied Optics, 44, 4102
- Cutri R. M., Skrutskie M. F., Van Dyk S., et al. 2003, 2MASS All Sky Data Release
- Dartois, E., et al. 1998, A&A, 338, L21
- Dickinson, M. et al., in prep.
- Downes D. et al., 1999, A&A, 347, 809
- Dudley. C. C. & Wynn-Williams, C. G. 1997, ApJ, 488, 720
- Dudley C. C., 1999, MNRAS, 304, 549
- Dunlop, J. S. et al. 2004, MNRAS, 350, 769
- Dunne, L., Eales, S., Edmunds, M., Ivison, R., Alexander, P., Clements, D. L. 2000, MNRAS. 315, 115
- Elvis, M., Wilkes, B. J., McDowell, J. C., Green, R. F., Bechtold, J., Willner, S. P., 1994, ApJS, 95, 1
- Fan, X., et al. 2004, AJ, 125, 1649
- Fan, X., et al., 2004, AJ, 128, 515
- Fernández-Soto, A., Lanzetta, K. M., Yahil, A., 1999, ApJ, 513, 34

- Frayser, D. T., et al., 2006, ApJ, 647, L9
- Geballe, T. R., Goto, M., Usuda, T., Oka, T., McCall, B. J. 2006, ApJ, 644, 907
- Genzel, R. et al. 1998, ApJ, 498, 579
- Gerakines P. A., Bray J. J., Davis A., Richey C. R., 2005, ApJ, 620, 1140
- Giavalisco M. et al., 2004, ApJ, 600, L93
- González-Alfonso, E., Smith, H. A., Fischer, J., Cernicharo, J., 2004, ApJ, 613, 247
- Greenberg, J. M., Li, A. Mendoza-Gomez, C. X., Schutte, W. A., Gerakines, P. A. & de Groot, M. 1995, ApJ, 455, L 177
- Hagen, W., Greenberg, J. M. & Tielens, A. G. G. M. 1983, A&AS, 51, 389
- Heger, A. & Woosley, S. E. 2002, ApJ, 567, 532
- Helou, G., Soifer, B. T., Rowan-Robinson, M., 1985, ApJ, 298, L7
- Hoogzaad S. N., Molster E. F., Dominik C., Waters L. B. F. M., Barlow M. J., de Koter A., 2002, A&A, 389, 547
- Huchra, J. P., 1977, ApJS, 35, 171
- Hughes D. H. et al., 1998, Nature, 394, 241
- Imanishi, M., Dudley, C. C., 2000, ApJ, 545, 701
- Imanishi, M., Dudley, C. C., Maloney, P. R., 2001, ApJ, 558, L93
- Imanishi, M., Maloney, P. R., 2003, ApJ, 588, 165
- Imanishi, M., Dudley, C. C., Maloney, P. R., 2006, ApJ, 367, 114
- Imanishi, M., 2006, AJ, 131, 2406
- Imanishi, M., Dudley, C. C., Maiolino, R., Maloney, P. R., Nakagawa, T., Risaliti, G. 2006, ApJ, submitted
- Jimenez et al. 2000, ApJ, 532, 152
- Kim, D.-C. & Sanders, D. B. 1998, ApJS, 119, 41
- Kim D.-C., Veilleux S., Sanders D. B. 2002, ApJS, 143, 277

- Klaas, U., Laureijs, R. J., Radovich, M., Schulz, B., Wilke, K., 2000, ISOPHOT Calibration Accuracies, SAI/1998-092/Dc, Ver. 4
- Klaas, U. et al. 2001, *A&A*, 379, 823
- Le, T., Dermer, C. D., 2006, *ApJ*, 661, 394L
- Leitherer, C. et al. 1999, *ApJS*, 123, 3
- Lis, D. C., Serabyn, E., Keene, J., Dowell, C. D., Benford, D. J., Phillips, T. G., Hunter, T. R. & Wang, N. 1998, *ApJ*, 509, 299
- Lisenfeld, U., Isaak, K. G., Hills, R. 2000, *MNRAS*, 312, 433
- Maloney, P. R. & Reynolds, C. S. 2000, *ApJ*, 545, 23
- McCutcheon, W. H., Sato, T. Purton, C. R. Matthews, H. E. & Dewdney, P. E. 1995, *AJ*, 110, 1762
- Mihos, J. C., Hernquist, L., 1996, *ApJ*, 464, 64
- Monet D., Canzian B., Harris H., Reid N., Rhodes A., Sell S. 1998, US Naval Obs. Flagstaff Station 1977, 1243
- Moore, M. H. & Hudson, R. L. 1992, *ApJ*, 401, 353
- Moshir M. et al. RAS Faint Source Catalogue, version 2.0
- Nenkova, M., Ivezić, Z., Elitzur, M., 2002, *ApJ*, 570, L9
- Nolta, M. R. et al. 2004, *ApJ*, 608, 10
- Nozawa, T., Kozasa, T., Umeda, H., Maeda, K., Nomoto, K., 2003, *ApJ*, 598, 785
- Osterbrock, D. E., 1993, *ApJ*, 404, 551
- Persson, S. E., Frogel, J. A., Aaronson, M., 1979, *ApJS*, 39, 61
- Pope, A., Borys, C., Scott, D. Conselice, C., Dickinson, M., Mobasher, B., 2005, *MNRAS*, 358, 149
- Riess, A. G. et al. 2004, *ApJ*, 607, 665
- Rigopoulou, D., Lawrence, A., Rowan-Robinson, M. 1996, *MNRAS*, 278, 1049
- Risaliti, G., et al., 2006, *MNRAS*, 365, 303

- Robson, I., Priddey, R. S., Isaak, K. G., McMahon, R. G., 2004, MNRAS, 351, L29
- Roche, P. F., Aitken, D. K., 1984, MNRAS, 208, 481
- Roussel, H., Helou, G., Beck, R., Condon, J. J., Bosma, A., Matthews, K., Jarrett, T. H., 2003, ApJ, 593, 733
- Sanders, D. B. 2000, AdSpR, 25, 2251
- Sander D. B., Egami E., Lipari S., Mirabel I. F., Soifer, B. T., 1995, AJ, 110, 1993
- Sanders, D. B. & Mirabel, I. F. 1996, ARAA, 37, 749
- Saunders, W., Rowan-Robinson, M., Lawrence, A., Efstathiou, G., Kaiser, N., Ellis, R. S., Frenk, C. S., 1990, MNRAS, 242, 318
- Schober, H., Koza, M. M., Tölle, A., Masciovecchio, C., Sette, F., Fujara, F. 2000, PhRvL, 85, 4100
- Schneider, R., Ferrara, A., Salvaterra, R., 2004, MNRAS, 351, 1379
- Scoville, N. Z. et al. 1991, ApJ, 366, L8
- Soifer B. T. et al., 1987, ApJ, 320, 238
- Soifer, B. T., Neugebauer, G., Matthews, Becklin, E. E., Ressler, M., K., Werner, M. W., Weinberger, A. J., Egami, E., 1999, AJ, 118, 2065
- Soifer, B. T., Neugebauer, G., Matthews, K., Egami, E., Weinberger, A. J., 2002, AJ, 124, 2980
- Smith, R. G. et al. 1994, MNRAS, 271, 481
- Spergel, D. N. et al. 2006, ApJ, submitted
- Spergel, D. N. et al. 2003, ApJS, 148, 175
- Spoon, H. W. W. et al. 2002, A&A, 414, 873
- Spoon, H. W. W., et al., 2006, ApJ, 638, 759
- Stockton, A., Canalizo, G., Maihara, T. 2004, ApJ, 605, 37
- Temi, P., Mathews, W. G., Fabrizio, B., 2005, ApJ, 622, 235
- Verma, A., Rowan-Robinson, M., McMahon, R., Efstathiou, A., 2002, MNRAS, 335, 574

- Wang, W.-H., Cowie, L. L., Barger, A. J. 2004, ApJ, 613, 655
- Weedman, D. W., et al. 2005, ApJ, 633, 706
- Willott, C. J., McLure, R. J., Jarvis, M. J., 2003, ApJ, 587, L15
- Whittet, D. C. B., Bode, M. F., Longmore, A. J., Adamson, A. J., McFadzean, A. D.,
Aitken, D. K., Roche, P. F., 1988, MNRAS, 233, 321
- Xilouris, E. M., Madden, S. C., Galliano, F., Vigroux, L., Sauvage, M., 2004, A&A, 416, 41
- Yun M. S., Reddy N. A., Condon J. J., 2001, ApJ, 554, 803

Fig. 1.— Upper Panel: Data from Imanishi & Maloney (2003) is reproduced for IRAS 00188-0856 together with a model (solid line) subsequently employed in the lower panel. The model consists of an $\alpha = 2$ (flux density $f_\nu \propto \nu^{-\alpha}$) power-law continuum to which absorption is applied together with an unabsorbed component which is a combination of an archival spectrum of M 82 (ISO SWAA11600319) and a blackbody of temperature 2500 K to represent additional stellar photospheric emission (displayed in the lower panel long-dashed line). The two absorption components used are: (1) a volatile admixture ($\text{H}_2\text{O}:\text{CO}=2:1$) of amorphous ice measured at 10 K (Hagen et al. 1983) and (2) the refractory EURECA-B curve presented by Greenberg et al. (1995). The effects of absorption by the refractory material are shown with the dot-dashed line and those of the combined volatile and refractory absorption with the dashed line. The volatile and refractory components have approximately equal contributions to the absorption at $3\ \mu\text{m}$ but the refractory component contributes little at the short wavelength edge suggesting that a volatile component is required. Lower Panel: The same model (solid line), now adjusted to lower optical depth in the refractory component to better match the $6\ \mu\text{m}$ absorption and with a smaller additive M 82 component is applied to longer wavelength data. Here, the effects of silicate absorption have also been included based on fig. 5 of Dudley & Wynn-Williams (1997) but oddly shifted to the red by about $0.6\ \mu\text{m}$ at $10\ \mu\text{m}$, perhaps owing to differing composition. The inset shows the effects of adding the spectrum of M 82 as in the upper panel and without this component in the model at all (bounding dotted lines). The spectral resolution of the model matches that of the data in the inset. The short-dashed line is an emission model described more fully in the text (Sec. 4.1). Data sources for IRAS 00188-0856 in descending order in the legend are from Imanishi & Maloney (2003); Monet et al. (1998); Cutri et al. (2003); Moshir et al. (1990); and Charmandaris et al. (2002). R and K' data are in rough agreement with the photometry given by Kim, Veilleux & Sanders (2002).

Fig. 2.— Highly processed data products from the ISO Archive (hpdp_05100540_2.tar and hpdp_65000608_2.tar with minimal ISAP post processing) are compared with a $43\ \mu\text{m}$ ice absorption feature derived from the spectrum of HD 161796 (also from the ISO archive: SWAA52100537). The diamonds and circles are data for Mkn 231 and IRAS 17208–0014 respectively. The solid lines are derived from the ISO SWS spectrum of HD 161796 using a single temperature (140 K) to estimate emissivity after the manner of Roche & Aitken (1984) and then converted to absorption. The inset is described in the text.

Fig. 3.— Observational data for IRAS 14348-1447 (filled circles) are plotted at their rest wavelength in Jy as reported by Klaas et al. (2001). Horizontal bars indicate filter passbands. The solid line shows an optically thin (in the FIR) ice emission model whose β parameter (100 and 300–900 μm) is ~ 2.3 as compared to ~ 1.9 for a bare (refractory) core. Adjustment of the core to smaller β would result in a smaller β for the mantled grain as well. In fitting the model data at 95 and 450 μm were matched and various mantle-to-core volume ratios were compared with photometry between these wavelengths. The dashed line reproduces the fit proposed by Klaas et al. (2001) which is quite optically thick in the FIR and has $\beta=2$.

Fig. 4.— Observational data for QSO J1154+5251 (filled circles and arrow) are plotted at their rest wavelength in mJy as reported by Bertoldi et al. (2003a) (3 mm); Bertoldi et al. (2003b) (1.2 mm); Robson et al. (2004) (850 and 450 μm); Beelen et al. (2006) (350 μm). The lines represent emission models. The dashed and dot-dashed are single temperature models using refractory and ice mantled dust respectively while the solid line two temperature ice model with colder ice obscuring warmer ice.

Fig. 5.— The observed frame 450-to-850 flux density ratio calculated for a series of emission models is plotted as a function of redshift together with 9 observed lower limits (large filled symbols), 34 observed upper limits (medium open symbols), and two detections (smallest symbols). Individual 450 μm source and detection identifications are given in the legend. The models, also in the legend, are more fully described in the text.

Fig. 6.— Brightness in mJy at the observed wavelength 450 μm is plotted as a function of redshift for a set of models. Four of the models are carried over from Fig. 5: The solid line represents 150 K ice, the triple dot dashed line, 50 K ice, the dot dashed line 30 K ice and the long dashed line 60 K refractory dust. A fifth model (short dashed line) is taken from the solid line in Fig. 4: 71 K ice is obscured by 24 K ice. Infrared luminosities for the models are constant as a function of redshift and are $2 \times 10^{13} L_{\odot}$: long-dashed, dot-dashed, and triple-dot-dashed lines, $2 \times 10^{14} L_{\odot}$: solid line, and $1 \times 10^{13} L_{\odot}$: short-dashed line. We remark that just as standard dust shows roughly redshift independent brightness at 850 μm , so too does T=50 K ice (triple dot dashed line) at 450 μm . The filled circle is QSO J1148+5251.

Fig. 7.— Observational data for HDF 850.1 (filled circles) are plotted for a rest wavelength and luminosity scale corresponding to a redshift of 12.6 and accounting for the effects of gravitational lensing by reducing the apparent luminosity by a factor of 3. The data, except for the Z band limit, are reported or summarized in Dunlop et al. (2004). The Z band limit is measured from GOODS ACS data (Giavalisco et al. 2004) by subtracting the image of the lensing galaxy from itself after a rotation of 180° . The limit is 2σ drawn from the weight image for an $0''.5$ aperture centered at the IRAM position (Downes et al. 1999) and corresponds to $Z - K' > 3.5$ (Vega). Data for the lensing source (filled diamonds) should be read relative to the HDF 850.1 data (filled circles) as the scalings in wavelength and luminosity do not apply. Here the $I - K'$ photometry are from Dunlop et al. (2004) while the $3.6\text{--}24\text{ }\mu\text{m}$ points are measured from GOODS IRAC and MIPS images (Dickinson et al. 2006). The IRAC data are $6''.0$ diameter aperture photometry subtracting an equal area outer annulus. The $24\text{ }\mu\text{m}$ datum is obtained through radial profile fitting after subtraction of a confusing source and is perhaps a 2.5σ measurement of $20\text{ }\mu\text{Jy}$. The dashed line is scaled ($z = 1.1$ wrt observed frame; Fernández-Soto et al. 1999) data for the elliptical galaxy NGC 1399 (Persson et al. 1979; Athey et al. 2002) and the triple-dot-dashed line is for the galaxy NGC 3928 (Huchra 1977; 2MASS; Xilouris et al. 2004) with the shaded region between them showing the age dependent range of mid-infrared flux suggested by models for elliptical galaxies reported by Temi et al. (2005). The models shown as solid lines are described more fully in the text.

Fig. 8.— The $850\text{ }\mu\text{m}$ brightness as a function of redshift is shown for three calculated SEDs. The solid line corresponds to the FIR SED shown in Fig. 1. The long-dashed line corresponds to an optically thin $T = 45$, $\beta = 1.2$ modified blackbody similar to the Scoville et al. (1991) fit for Arp 220. The short-dashed line corresponds to the FIR SED shown in Fig. 7 all normalized to the FIR luminosity of IRAS 00188-0856. The arrows for the solid, dot-dashed, and dashed lines indicate redshifts for HDF 850.1 estimated using Fig. 1, Dunlop et al. (2004), and Fig. 7 respectively. The numbers at the right are a conversion of the vertical scale for the gravitational lens amplification factor of three estimated for HDF 850.1.

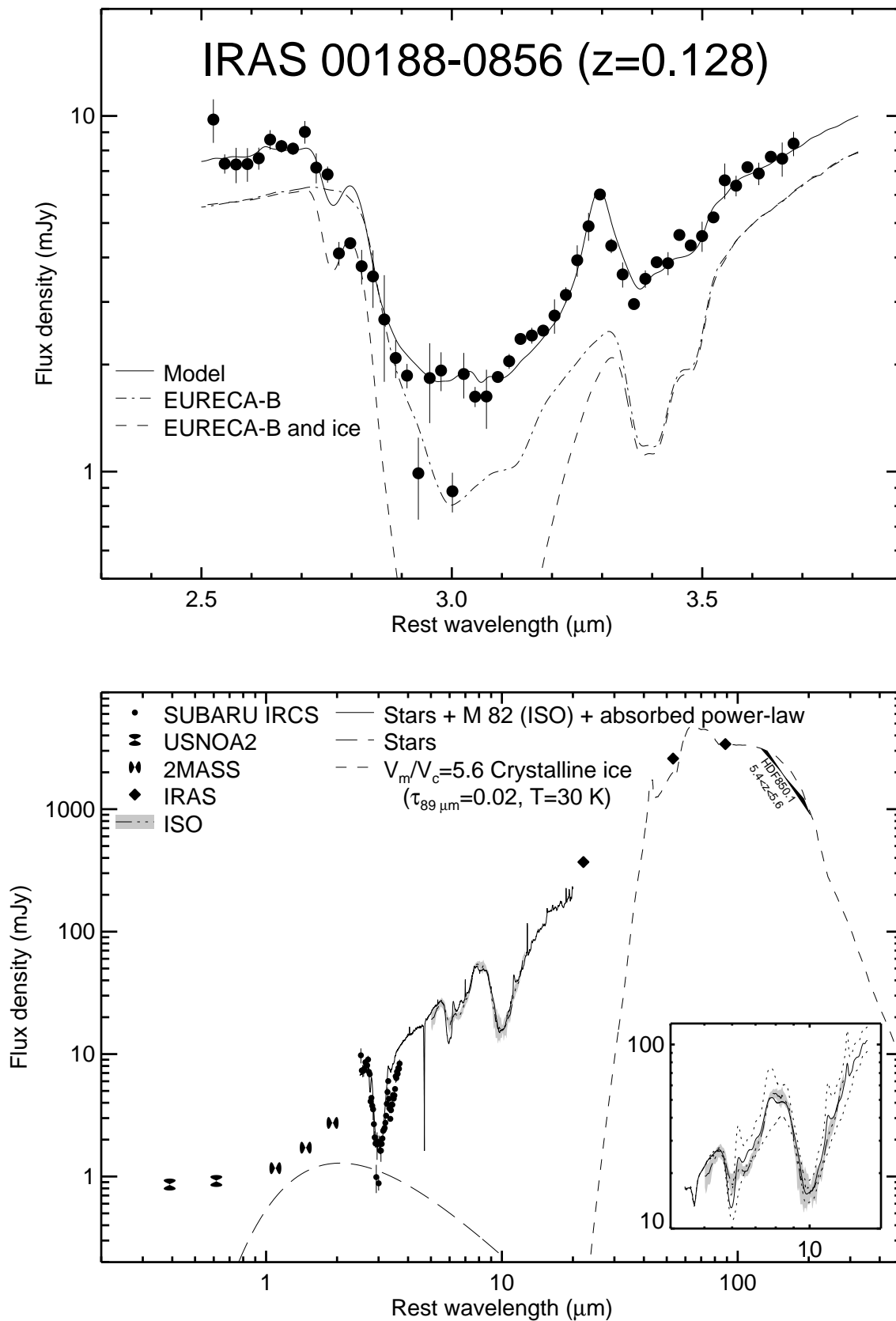


Fig. 1.—

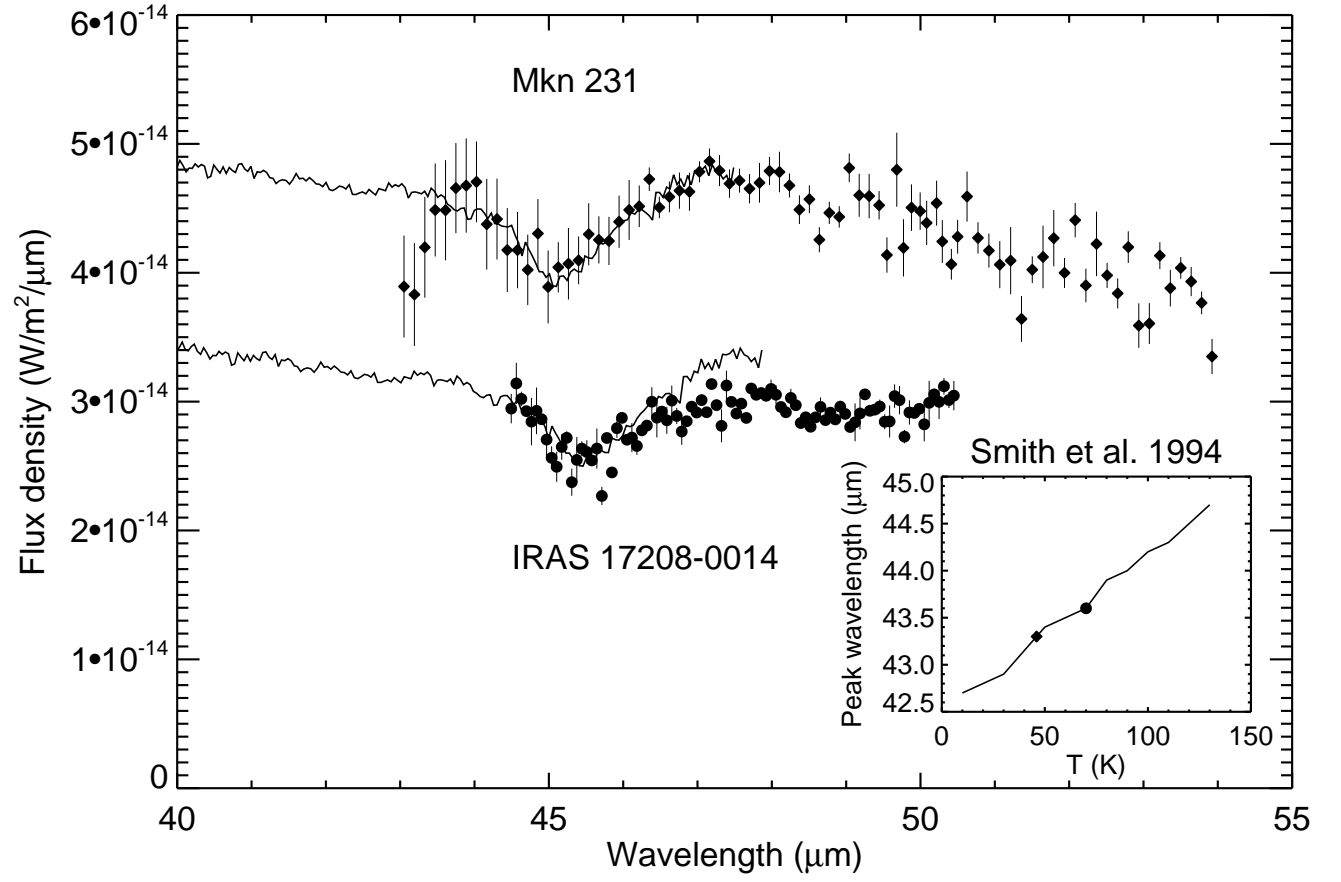


Fig. 2.—

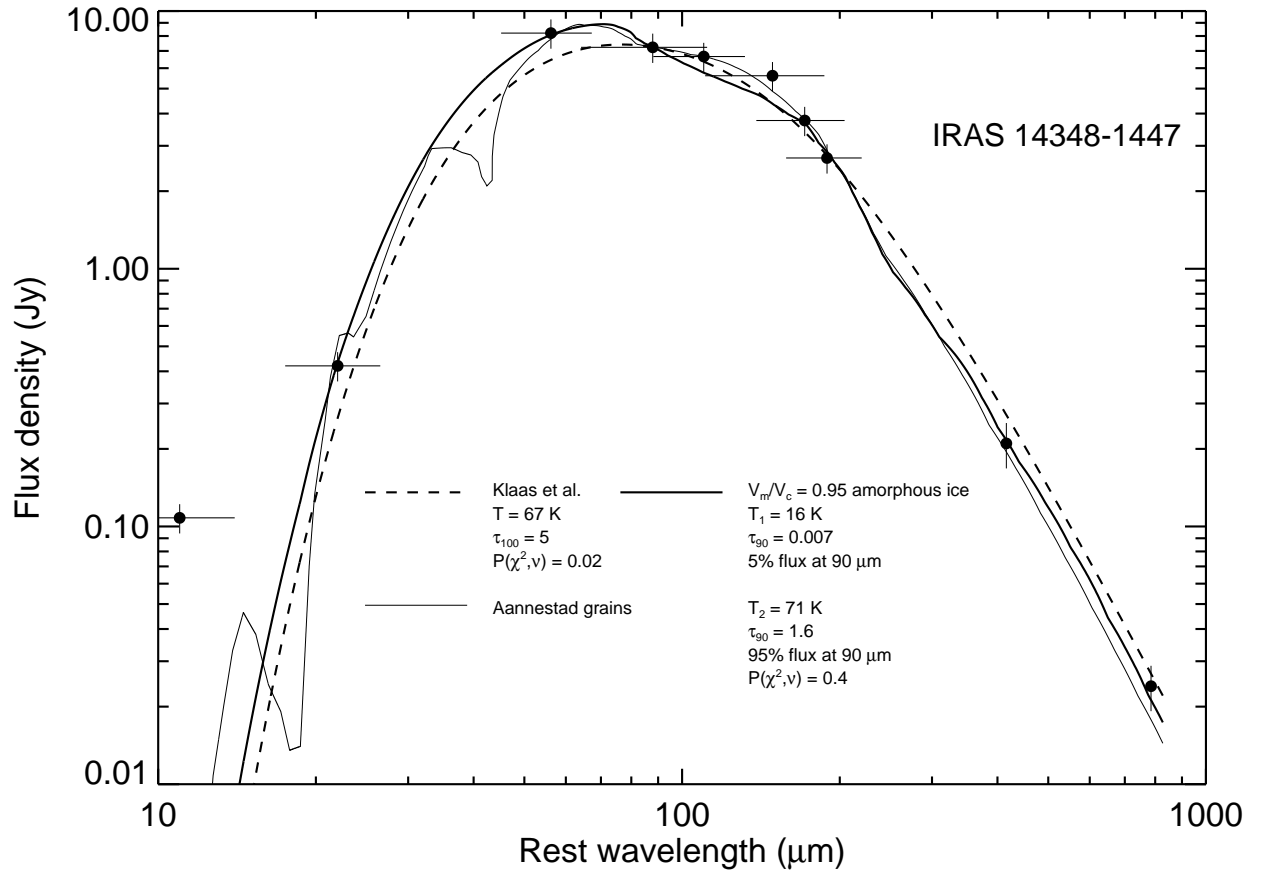


Fig. 3.—

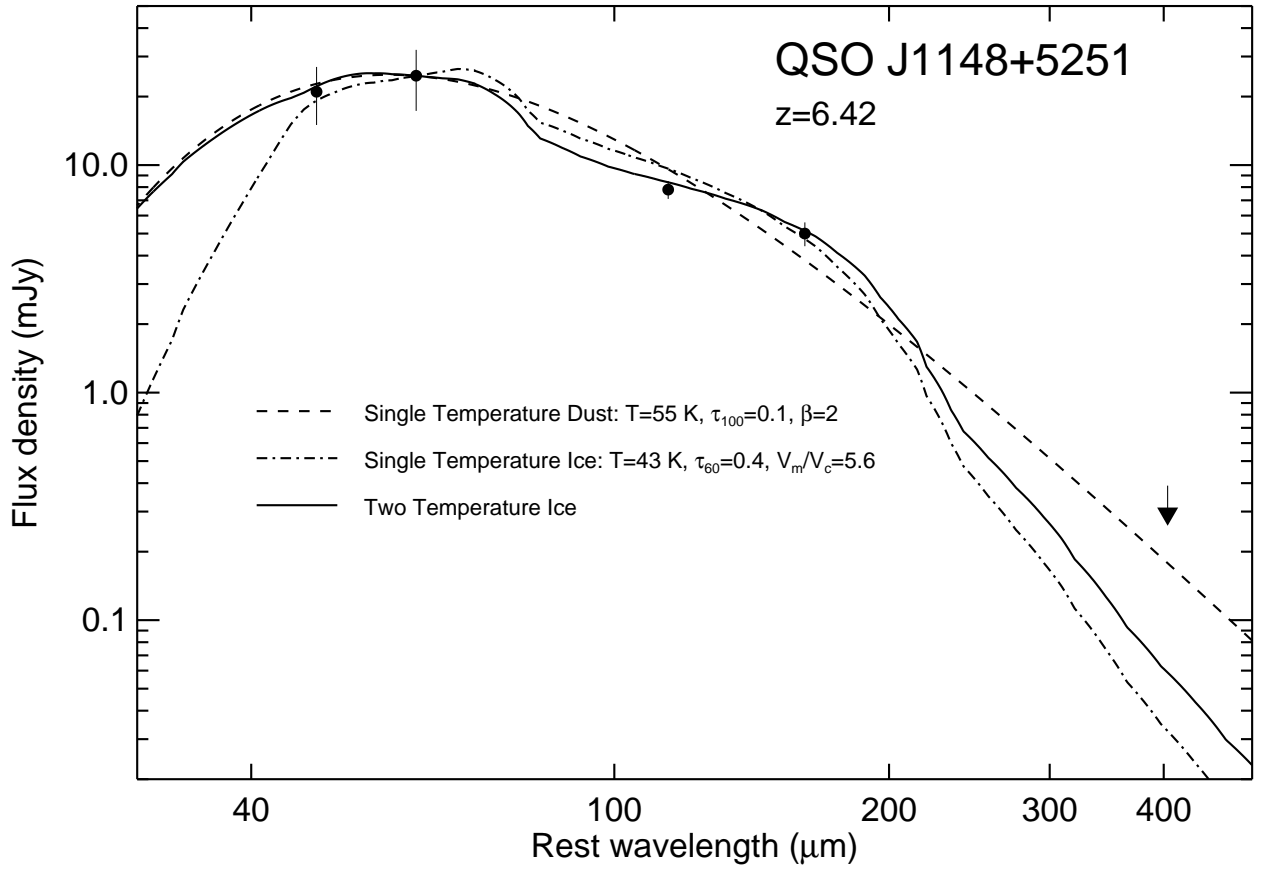


Fig. 4.—

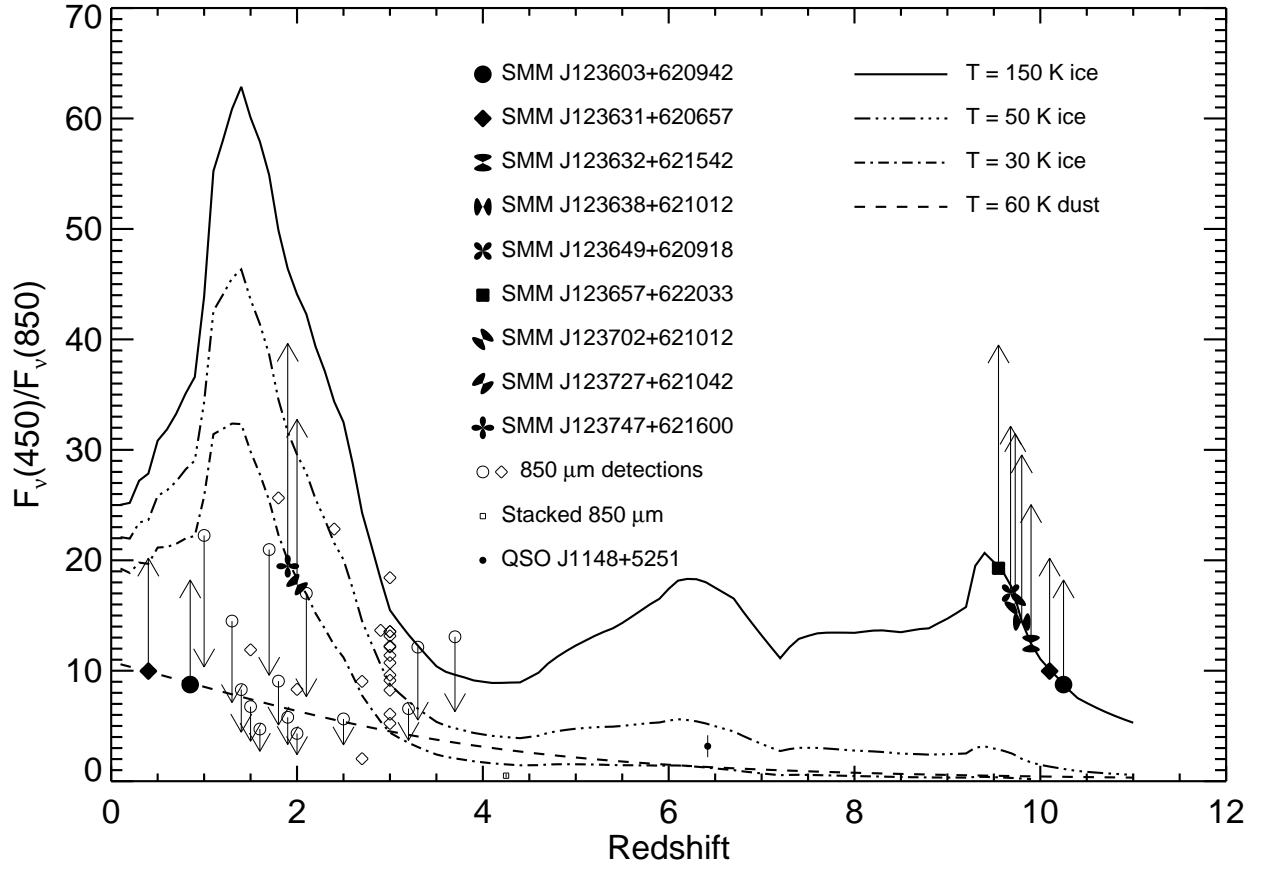


Fig. 5.—

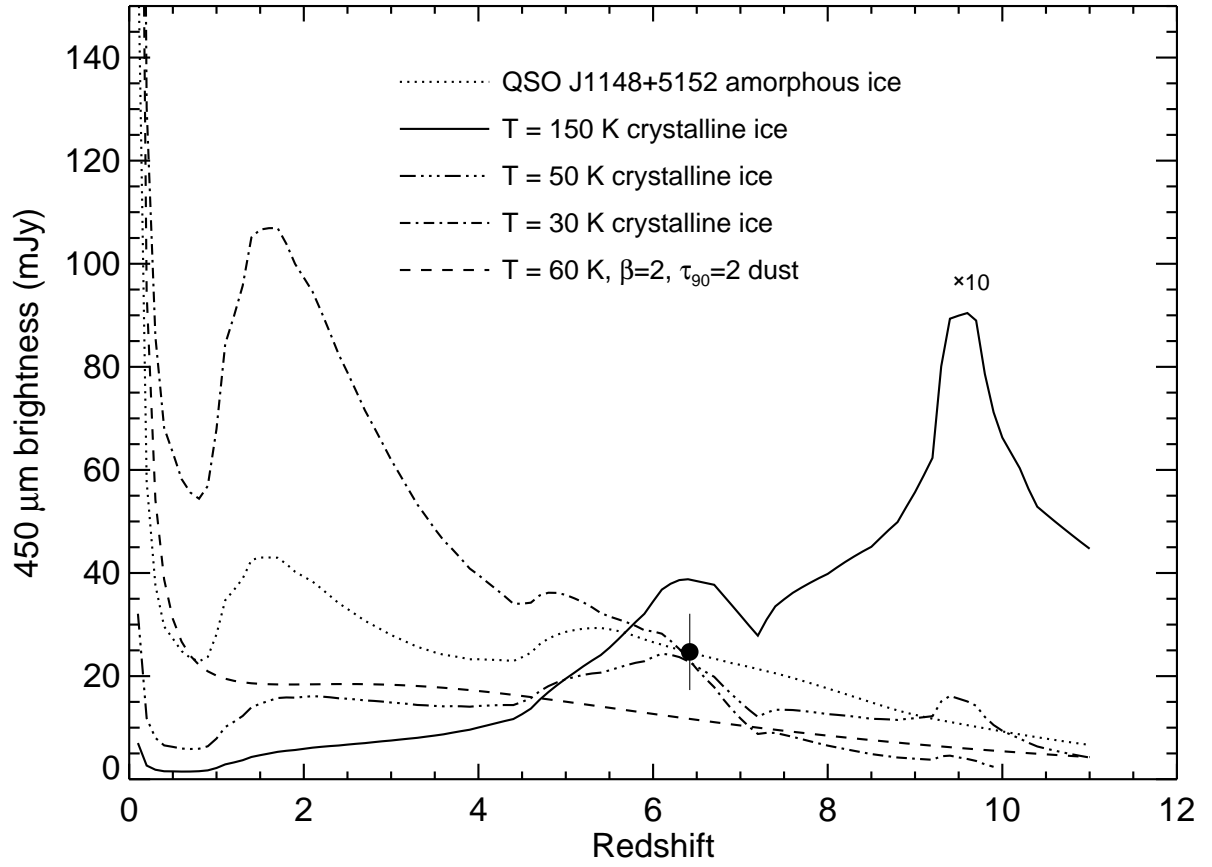


Fig. 6.—

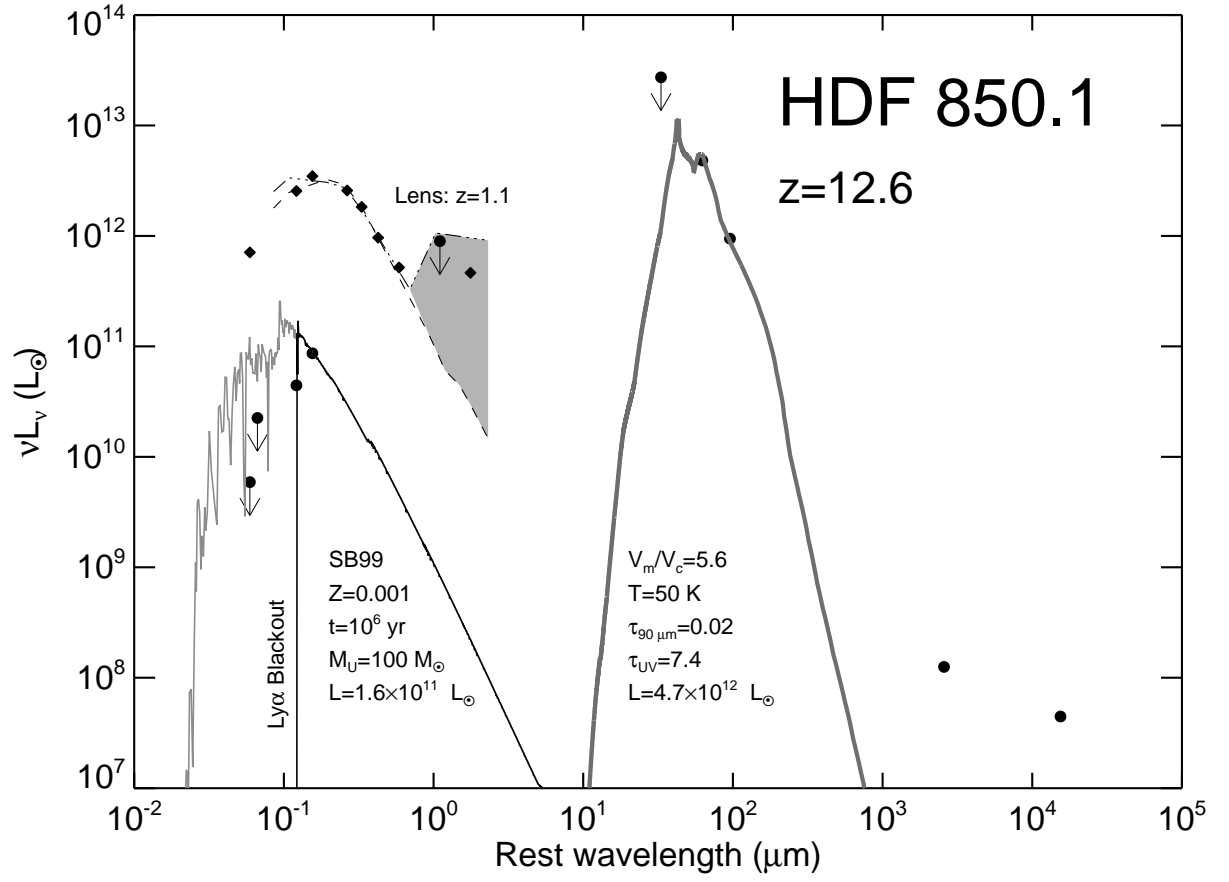


Fig. 7.—

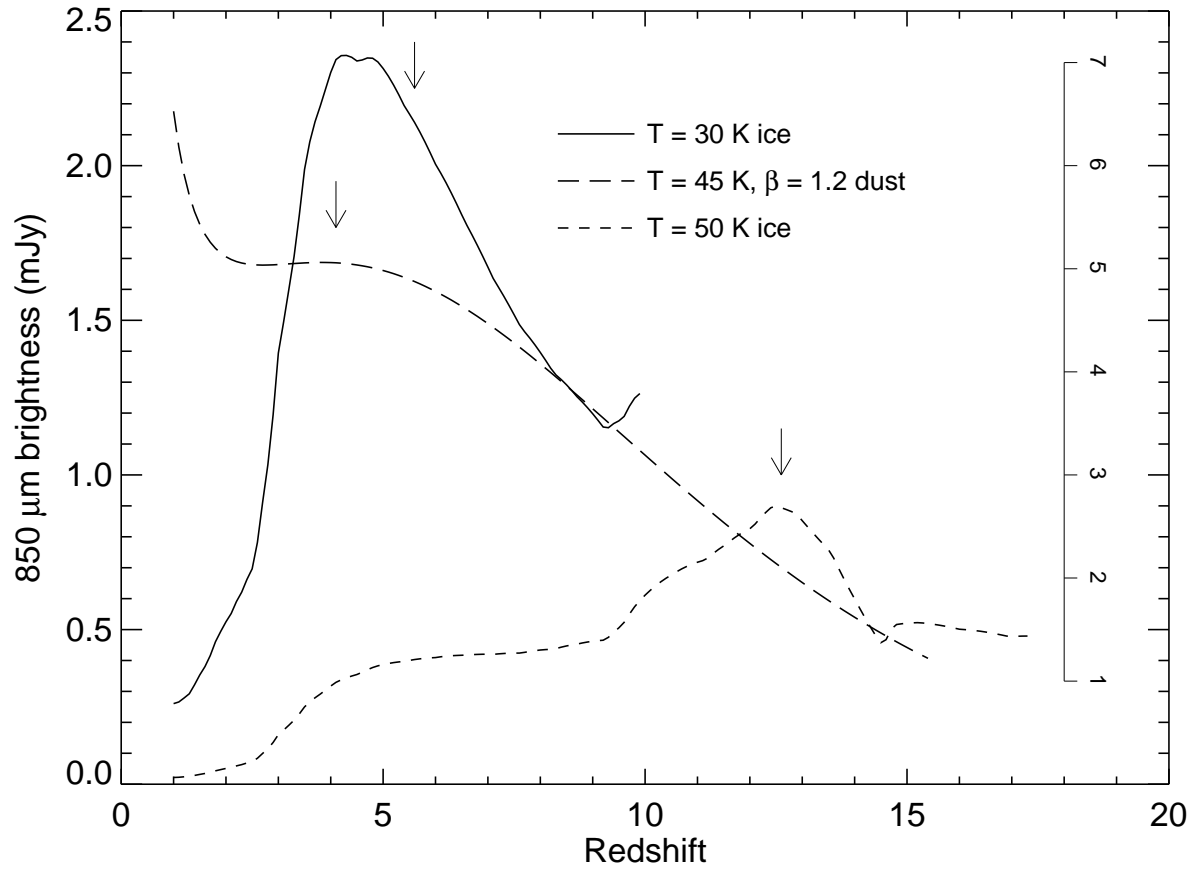


Fig. 8.—